SubZero: A Sea Ice Model with an Explicit Representation of the Floe Life Cycle

Georgy E. Manucharyan and Brandon P. Montemuro

School of Oceanography, University of Washington, Seattle, WA

Key Points:

- This paper is a non-peer reviewed preprint submitted to EarthArXiv and has been submitted for publication to the Journal of Advances in Modeling Earth Systems (JAMES) for peer review. Subsequent versions of this manuscript may have slightly different content.

Corresponding author: Georgy Manucharyan, `gmanuch@uw.edu`

Abstract

Sea ice dynamics span a wide range of scales and exhibit granular behavior as individual floes and fracture networks become evident at length scales O(10–100) km and smaller. Existing floe-scale sea ice models use bonded elements of predefined simple shapes like disks or tetrahedra to represent more complex floe geometries. However, floe-scale modeling remains challenging due to its typically high computational cost and difficulties in reconciling the idealized nature of discrete elements with complex floe-scale observations. Here we present SubZero, a conceptually new sea ice model geared to explicitly simulate the lifecycles of individual floes by using complex discrete elements with time-evolving shapes. This unique model uses parameterizations of floe-scale processes, such as collisions, fractures, ridging, and welding, to bypass the high computational costs of resolving intra-floe bonded elements. We demonstrate the novel capabilities brought by the SubZero model in idealized experiments, including the summer-time sea ice flow through the Nares Strait and a winter-time equilibration of floe size and ice thickness distributions. The SubZero model could provide a valuable alternative to existing discrete element and continuous sea ice models for simulations of floe interactions.

1 Introduction

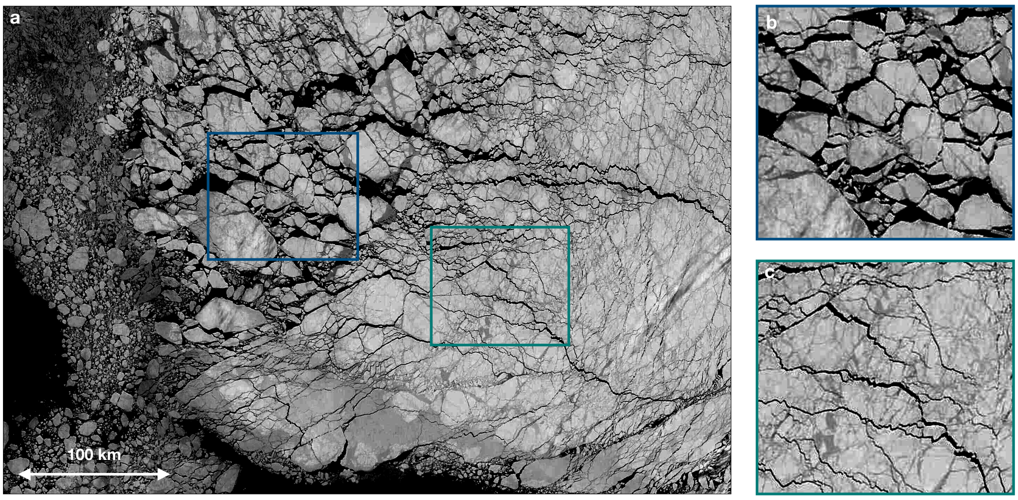

Figure 1. Example of the summertime sea ice in the Western Arctic Ocean, near Banks Island demonstrating its granular discontinuous nature and spatial heterogeneity. **(a)** A filtered reflectance image from the NASA WorldView website encompassing a region about 550 by 350 km in size bounded by 71–76^{o}N in latitude and 126-137^{o}W in longitude, taken on May 17th, 2021. The image filtering included making it gray scale and adjusting the level curves to highlight the fracture network and individual floes. **(b,c)** Zoomed-in view of the rectangular regions about 100 by 100 km in size as denoted in **(a)**.

Sea ice motion at relatively large scales, O(100 km), is commonly represented in climate models using continuous rheological models (Hibler, 1979; Hunke & Dukowicz, 1997; Rampal et al., 2016). However, at relatively small scales, O(10–100) km and smaller, sea ice can be viewed as a granular material consisting of a collection of interacting floes (D. Rothrock & Thorndike, 1984; Zhang et al., 2015; Stern et al., 2018). The discrete floe dynamics are particularly pertinent in marginal ice zones where interacting floes are distinctly observed in satellite images, and sea ice resembles granular material (Fig. 1).

In consolidated pack ice, floes can be frozen to each other (welded) but externally forced large-scale sea ice motion can occur due to frequent anisotropic fractures and deformation (Hibler III & Schulson, 2000; Hutchings et al., 2011). Since specific floe configurations, their mechanical properties, and existing fracture networks are expected to affect the short-term evolution of sea ice, it is desirable to represent these features in models explicitly.

While continuous models can run at very high resolutions, the assumptions under which they are applicable formally require the grid box size to be significantly larger than the characteristic floe size such that floe interactions can be represented statistically. Nonetheless, high-resolution numerical simulations can generate discontinuities that resemble observed linear kinematic features (Hutter & Losch, 2020; Mohammadi-Aragh et al., 2020; Mehlmann et al., 2021; Hutter et al., 2022). But despite the major progress of continuous modeling of large-scale sea ice and the ongoing developments in pushing their applicability limits by increasing the resolution, the rheological models are not meant to represent the scales of motion at which individual floes start to affect dynamics. Hence, the validation against floe-scale observations for continuous models is only possible using statistical characteristics or large-scale sea ice motion because the rheological parameters parameterize cumulative effects of floe interactions. Consequently, direct comparisons of continuous models to remote sensing or field observations of individual floe behavior are challenging.

Alternatives to continuous rheology models are Discrete Element Models (DEMs), developed initially in the context of granular assembles and rock dynamics (Cundall & Strack, 1979; Potyondy & Cundall, 2004). DEMs represent media as a collection of a large number of colliding and/or bonded elements of specified shapes and contact laws and hence are typically computationally demanding. Since the continuous equations of motion are often unknown, DEMs resort to specifying the interaction laws between its elements and strive to calibrate them using micro-scale observations. Another way of simulating fluid motion with known rheology is the Smoothed Particle Hydrodynamics approach that also simulates particle motion but the laws of their interaction are strictly derived from the continuous fluid rheology (Monaghan, 1992; Gutfraind & Savage, 1997; Lindsay & Stern, 2004). As such, DEMs present a more general class of models that could simulate media for which corresponding macro-scale rheology might not exist but the interaction laws between its particles could be constrained from observations.

With increasing computational capabilities and the emergence of comprehensive field and remote sensing observations at the floe-scale, the DEM approach has been adapted for modeling the discontinuous sea ice dynamics and continues to be revisited and improved (Hopkins et al., 2004; Wilchinsky et al., 2010; Herman, 2013, 2016; Kulchitsky et al., 2017; Damsgaard et al., 2018; Liu & Ji, 2018; Tuhkuri & Polojärvi, 2018; West et al., 2021). At engineering scales, below about O(10-100) m, sea ice DEMs have implemented a bonded particle model (Liu & Ji, 2018; Tuhkuri & Polojärvi, 2018). At these scales, the models could be cross-validated with laboratory experiments, specialized field observations, and measurements of stress from structure-ice interactions, including ships. Sea ice DEMs have also been used exploring idealized processes, including jamming and ice bridge formation in straits (Damsgaard et al., 2018) and wave-floe interactions (Herman et al., 2019). At larger regional scales, up to a few 100 km, the (Hopkins et al., 2004; Wilchinsky et al., 2010) model and its recent modification that utilizes level sets to compute collisions (Kawamoto et al., 2016) has been adapted for regional simulations Nares Strait (West et al., 2021). Siku model (Kulchitsky et al., 2017) is capable of simulating the formation of basin-scale linear kinematic features in the Beaufort Gyre associated with the coastal features. DEMs are computational demanding and their use in coupled Earth system models is challenging but a prototype of such a model (DEMSI) is currently under development (Turner et al., 2022).

Existing sea ice DEMs [see Tuhkuri and Polojärvi (2018) for the review] follow a conventional approach of using simple pre-defined shapes for the elements, e.g., points or disks (Herman, 2013; Damsgaard et al., 2018; Chen et al., 2021a), polygons (Kulchitsky et al., 2017) or tetrahedra (Liu & Ji, 2018). However, observations demonstrate that floes range dramatically in shapes and sizes (Fig. 1) and evolve in time subject to a variety of processes like fractures, rafting and ridging, lateral growth/melt, welding, etc. Hence, using pre-defined element shapes brings some ambiguity about what elements and bonds between them physically represent. Are elements supposed to approximate the behavior of aggregates of floes (similar to what continuous rheological models are assuming), or perhaps they are representing bonded constituents of floes or some other metric of a sea ice state? Without a robust understanding of what a DEM element represents, it is difficult to search for direct correspondence between the state variables of the DEM and the observed sea ice. These are challenging questions, and the answers depend on the modeling philosophy because sea ice is a multi-scale media where grains are not well defined.

This manuscript presents a conceptually new discrete element approach to sea ice modeling that relies fundamentally on using elements with evolving boundaries to more realistically represent the floe life cycle. Our goal is to develop a model that could be used in conjunction with floe-scale satellite and in situ observations for floe-scale sea ice predictions and process studies. While the ice floe model consists of several mechanical and thermodynamic components, our focus is on developing a set of floe interaction rules that could lead to realistic sea ice mechanics, including distributions of floe sizes, thicknesses, and shapes. In contrast with existing sea ice DEMs, our approach is based on floes conceptualized as complex-in-shape time-evolving elements instead of specifying a large number of stiffly-bonded simple elements to represent floes. We argue that the model capability of developing floe shapes naturally, due to specific physical processes at play, might bring us closer to direct model validation with floe-scale observations. The numerical implementation of our proposed method is publicly available as the SubZero sea ice model (Manucharyan & Montemuro, 2022). Below, we provide the model formulation and present a few idealized simulations to showcase the novel capabilities.

2 SubZero model philosophy

In contrast with existing sea ice DEM methods, our sea ice DEM simulates the motion of elements that change their shapes, much like the observed sea ice floes do during interactions with other floes or boundaries. Crucially, the ability of model elements to change shape is not simply an additional improvement over existing DEMs that use fixed element shapes but something that leads to fundamentally different dynamics of floe interactions. Specifically, closely packed non-convex elements in our model can lead to interlocking behavior: a group of rigid floes cannot substantially move relative to each other except when they are allowed to fracture or in a degenerate case of low concentration. For the tightly packed interlocked floes, the motion can only occur if floes undergo area-reducing processes such as deformations induced by micro- and macro-scale fractures (for example, ridging/rafting). Consequently, virtual bonds between the interlocked elements are not entirely necessary as their role is partially transferred towards parameterizations of floe fractures and other processes that change the shape of individual floes. We hypothesize that a DEM formulation based on floe shape evolution would make the model less computationally expensive and comparisons with observed floes less ambiguous.

The increased complexity of floe interaction physics is the trade-off for using elements with freely evolving shapes. Floes undergo many processes that affect their shapes, including fractures, ridging, and welding, making them highly non-convex. In addition, the fracture process, which is essential to the model dynamics, rapidly increases the number of floes. To avoid an explosion of the number of floes in a model, it is necessary to

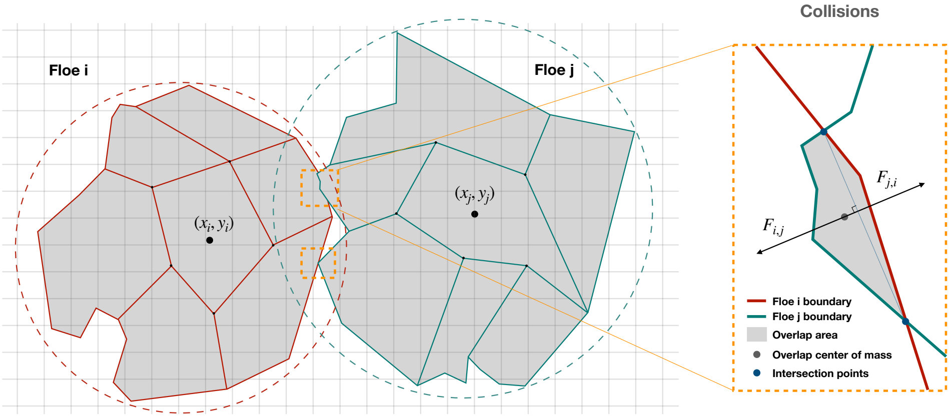

Figure 2. Example of two colliding floes outlining the corresponding normal collision forces appearing at the overlap areas. The bounding circles are shown for both floes and are used to determine if any two floes could be potentially colliding. Each floe could be composed of several rigidly-connected polygonal sub-floes if a more accurate floe-fracture model is needed. An example Eulerian grid that can be used for coupling with the oceanic and atmospheric model is shown with gray lines.

model only sufficiently large floes and treat sufficiently small floes as unresolved. Conventional DEMs can also generalize floes as a set of fixed-shaped elements that are bonded together, but the difference with our SubZero model is that by representing the complex floe shapes by their polygonal boundaries, it is not needed to simulate the interactions of elements covering its surface area. In other words, the trade-off in representing floes is between using a large number of simple fixed-shape elements with simple interaction rules versus representing it with a single complex-shaped polygon and complex physics describing its shape changes upon interactions with other floes. While using concave shape-changing floes as elements in a sea-ice DEM may lead to improved realism of simulations, it also creates new challenges in numerical integration and parameterizations of floe-scale physics that we address below.

3 Dynamical core of the SubZero model

Below we describe the dynamical core components of the model, with each component representing a relatively basic representation of key processes. Our modeling philosophy envisions that various model components will be improved by a broad sea ice research community based on observational, experimental, modeling, and theoretical studies.

3.1 Floes as polygons with changing boundaries

Motivated by observations of sea ice fracture networks and floe boundaries that appear piece-wise linear (Figure 1), we choose to use the polygonal representation of floes. The model homogenizes sea ice properties, such as the thickness within the floe, such that its polygonal shape defines the center of mass, total volume, and moment of inertia. The floes (i.e., their vertex coordinates) are translated following the velocity and angular velocity of the floe, which are calculated using the momentum and angular momentum equations written for individual floes (Section 3.3). The model has the capability

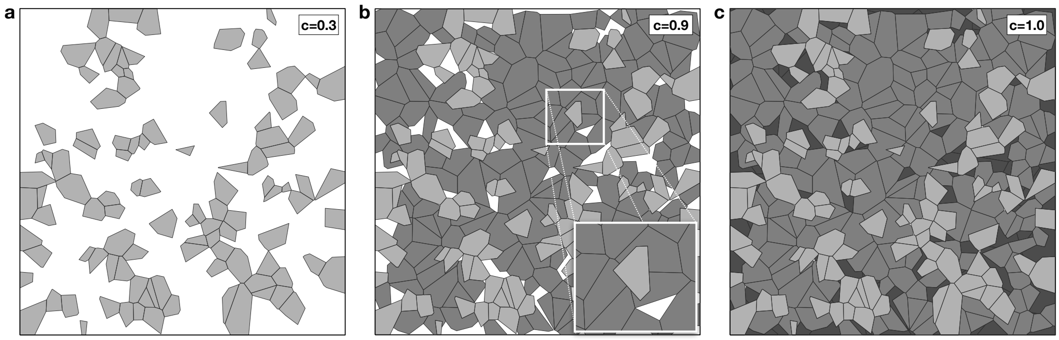

Figure 3. The initial state of the model achieved using the floe packing algorithm that incrementally increases the number of floes to match the desired mean sea ice concentration. Panels **(a-c)** correspond to 30%, 90%, and 100% sea ice coverage. Note that all floes are non-overlapping, and new floes are created in open areas without affecting the old floes. This creates non-convex floes that are interlocking due to each other, an example of which is shown in the panel **b** inset.

of splitting floes into rigidly connected sub-floes to keep track of floes that were ridged and/or welded together, with each sub-floe carrying its own properties, like thickness. However, this configuration is computationally demanding, and we expect it to be used when high-resolution information about intra-floe variability and floe fractures is needed. The basic version of the model does not keep track of the sub-floes and homogenizes floe characteristics after processes like welding.

While convex element shapes lead to dramatic simplifications in calculations of the collision forces, our model uses convex floes for better realism. Such crucial processes as floe fractures, welding, and ridging are in no way restricted to preserve the convex nature of the floes. In addition, creating new floes in complex empty areas between existing floes becomes a much simpler task when convex floes are used, allowing an arbitrarily-high concentration to be achieved without substantially modifying the floe-size distribution of existing floes.

The SubZero model could technically be reduced to a conventional DEM that uses bonded particles of fixed convex shapes. However, in winter-time simulations, wherein our model element shapes are allowed to evolve in time, the model state ends up being composed of highly complex and packed floes that are interlocked with each other. The interlocking behavior for complex-shaped polygons ensures that they are perfectly bonded, and the only plausible way to move this system is to generate a set of fracture/ridging/rafting events that could split a sufficient amount of floes from each other, creating some open area to allow motion. As a result, having virtual bonds between floes is not entirely necessary, as their role is transferred to such parameterizations as fractures/ridging/rafting that change the shapes of floes and reduce the sea ice area. Nonetheless, the bonds are necessary for more complex configurations of our model that can resolve dynamics within individual floes by splitting them into bonded sub-floes. Such configurations bring more detail to resolving the stress/strain within the floes, which may be relevant for predictions of processes like fractures occurring at a subset of floes in the location of interest like field camps or ship/submarine paths.

3.2 Creation of new floes and packing algorithm

Two primary scenarios call for the creation of new sea ice floes. First, at the beginning of a run, it is necessary to define the initial state of the floes corresponding to a designated sea ice concentration. Second, new floes to be created to fill the open space around existing floes if required by the thermodynamic criteria. New floes are created by the packing algorithm that requires specifying a target concentration for the entire domain (see an example in Figure 3) or by inputting a 2D matrix that specifies the desired spatially-varying concentration on a specified Eulerian grid.

The packing algorithm is designed in the following way. First, it identifies the space unoccupied by existing floes using polygonal operations like unions and differences. Then, the identified region is broken up into polygons using Voronoi tessellation and ensuring that each added new floe is not overlapped with existing ones by cutting the overlap region if it exists. These non-overlapping floes are added until a targeted concentration is reached. Control on the characteristic sizes of the floes exists by prescribing the number of points used for Voronoi tessellation. The new floes are then added to the floe structure that carries all floe parameters. The initialized floe velocities match the ocean velocity. However, the new floe velocity could also be set to zero in most circumstances as the floe velocity has a relatively short adjustment timescale to the external forcing. The packing algorithm is time-consuming and hence is not used at every timestep but with a specified frequency. The thickness of newly created floes is related to the time separation between packing events and on the heat fluxes received by the sea ice:

$$h_0 = \sqrt{\frac{2k\Delta t N_{pack}(T_o - T_a)}{\rho_{ice} L}}, \tag{1}$$

where k is the thermal conductivity of the surface ice layer, Δt is the time step during a model run, N_{pack} is the time steps between floe creation events, L is the latent heat of freezing and has units of Joules per kilogram, T_a is the temperature at the ice/air interface, and T_o and is the temperature at the ice/ocean interface (Cox & Weeks, 1988). The values used in SubZero are provided in Table 1.

3.3 Floe momentum and angular momentum evolution

Each floe in the model is treated as a rigid body with its center of mass $\mathbf{X}_i$ accelerating due to internal and external forces while its angular velocity Ω_i responds to the torques:

$$\begin{aligned} m_i\ddot{\mathbf{X}}_i &= \iint_{A_i} (\tau_{\mathbf{ocn}} + \tau_{\mathbf{atm}})\, dA + \sum_{j\neq i;k} \mathbf{F}^k_{ij} + \bar{\mathbf{f}}_i, \\ I_i\dot{\Omega}_i &= \iint_{A_i} (\mathbf{r} - \mathbf{X}_i) \times (\tau_{\mathbf{ocn}} + \tau_{\mathbf{atm}})\, dA + \sum_{j\neq i;k} (\mathbf{R}^k_{ij} - \mathbf{X}_i) \times \mathbf{F}^k_{ij} + \bar{g}_i. \end{aligned} \tag{2}$$

Here, indices i and j denote different floes and k enumerates their contact points as several of those could exist for non-convex floes; m_i, I_i, A_i are floe mass, moment of inertia and area; $\tau_{\mathbf{ocn}}$ and $\tau_{\mathbf{atm}}$ represent kinematic stresses from ocean and atmosphere; $\mathbf{F}^k_{ij}$ and $\mathbf{R}^k_{ij}$ are the interaction forces and coordinates of the k^{th} contact point for colliding i^{th} and j^{th} floes (land is conveniently treated as a stationary floe); and $\bar{\mathbf{f}}_i, \bar{g}_i$ are average forces and torques due to interactions with unresolved small-scale floes. The kinematic stresses from the ocean and atmosphere are calculated using a Monte Carlo integration technique. The location of these randomly distributed points to evaluate the various integrands is determined when the floe shape is initialized with the user prescribing the number of points. These locations are used when updating the trajectory of a floe by calculating the ice velocity, wind velocity, and ocean velocities to evaluate the stresses. Other body forces such as the Coriolis and sea surface tilt forces can also be turned on and computed the same way as torques. For simplicity, and given the lack of developed parameterizations, the basic version of the model does not include the forces and torques from unresolved floes, but later versions would include stochastic representations of the impact of unresolved floes on the dynamics of the resolved floes. Collision forces, $\mathbf{F}_{ij}$, consist of elastic (normal) and frictional (tangential) components which correspondingly are directed along and perpendicular to the line of contact between the two floes. In addition to shape-conserving interactions, the model includes a criterion for floe mergers (welding), ridging, as well as fractures leading to the creation of new smaller floes. Like continuous sea-ice models, the floe model is also limited in its effective resolution by imposing the minimum floe size to bound the total number of elements. This minimum floe size is a parameter that could vary depending on the type of sea ice in a given region, on the physical problem under consideration, and on available computing resources.

3.4 Contact forces between the floes

3.4.1 Detection of contact points

Each floe has a bounding circle associated with it, with the radius corresponding to the distance from its center of mass to the furthest vertex of its boundary. The bounding floe radii are then used to identify pairs of floes that could be potentially interacting. The polygons of the potentially interacting floes are copied into the memory for each of the floes to enable parallel computation of more complex polygonal operations to determine if the floes are actually overlapping and calculating the collision forces. Note that the floes are considered rigid (non-deformable) bodies, but we allow a small numerical overlap between the floes to exist in order to compute collision forces that depend on the geometry of the overlap area.

3.4.2 The normal direction at a contact point

The desired capability of simulating collisions between complex-shaped floe translates into some ambiguity in defining the normal and tangential directions at the contact points, which isn't present for simple convex shapes like circles. For non-convex polygons, two issues need to be addressed. First, there can be multiple contact points between two non-convex floes, and the forces associated with each need to be resolved separately. Second, when sufficiently large forces are driving the floes, the overlap area in some contact points can be of very complex shape such that it isn't clear how to define the directions of the collision forces. Here, we define the normal direction in the following way (Feng et al., 2012). First, at each contact point, the floe polygons intersect each other at two points, and we store the mid-point between them. Second, we calculate the center-of-mass position of the overlap area. The normal force is defined as pointing from the center of mass of the overlap area towards the mid-point of the polygon intersections. Finally, a check is made to ensure the overlap area would be reduced if the floes are being displaced in the direction of the corresponding normal forces; the normal direction is flipped if the check fails, which occurs in very rare marginal cases with complex shapes of the overlap areas.

3.4.3 Normal forces

Each floe has a center of mass and the maximum radius associated with it that are first used to sort out potentially interacting floe pairs. Afterward, an algorithm is used to determine the geometry of the overlapped area and the corresponding forces and torques. An energy-conserving contact algorithm (Feng et al., 2012) is used. The floe collision rules are based on simple physical laws for inelastic collisions of rigid bodies (Hopkins et al., 2004; Kulchitsky et al., 2017; Wilchinsky et al., 2010). For computational reasons, some small overlap area between the contacting floes is allowed to develop in order to define the normal and tangential forces at each contact point. Note that concave floes can have multiple contact points (see an example in Figure 2), with forces and torques at each of the contact points being computed separately. The normal forces depend on the relative location of the floes, being proportional to the overlap area at each contact location with the proportionality constant K and the size of the floes. For a given interaction force, increasing the parameter K decreases the overlap area between the floes to the extent that they start to appear like rigid bodies; however, this occurs at the expense of having to use a relatively small time interval to accurately resolve the collision forces. The parameter K could be taken to be as large as possible depending on the computational capabilities and the desired accuracy of collisions. However, keeping it finite brings a physical meaning that the floes are elastic and could have deformation expressed in the form of a finite overlap region between the flow and a general decrease of the overall area in the domain under compression. The equation for the normal force is

$$\mathbf{F}^k_{ij,n} = KA\mathbf{n}^k_{ij}, \tag{3}$$

where A is the overlap area and $\mathbf{n}^k_{ij}$ is the normal direction at the k^{th} contact point between the i^{th} and j^{th} floes. Note that for non-convex elements, there could be multiple contact points, and hence k could be greater than one. K can be found through the equation

$$K = \frac{E_i h_i E_j h_j}{E_i h_i r_j + E_j h_j r_i}, \tag{4}$$

where E is an elasticity value, h is the thickness, and r quantifies the floe size ($r_i = \sqrt{Area_i}$). The values used in SubZero are provided in Table 1. If there is an individual floe interacting with a non-deformable boundary ($E \to \infty$) then the equation simplifies to

$$K = \frac{E_i h_i}{r_i}. \tag{5}$$

3.4.4 Tangential forces

The frictional tangential force is proportional to the normal force and is associated with the average tangential velocity difference between the floes at the contact location (Cundall & Strack, 1979; Chen et al., 2021b). The basic frictional force model defines a coefficient of static friction and a smaller coefficient for the kinetic friction, taking the force to be proportional to the normal force only.

For this model, when the floes are in motion, the adjustment for the frictional laws is proportional to the velocity difference between the two floes, the time step, and the chord length. It is given by

$$|\mathbf{F}^k_{ij,t}| = c^k_{ij} G v^k_{ij} (\Delta t) |\mathbf{F}^k_{ij,n}| \mathbf{t}^k_{ij}, \tag{6}$$

where G is the shear modulus. The values used in SubZero are provided in Table 1. The velocity v^k_{ij} gives the difference between the two floes and is given by

$$v^k_{ij} = \left[\left(\mathbf{v}_j + \omega_j \times \mathbf{r}^k_j \right) - \left(\mathbf{v}_i + \omega_i \times \mathbf{r}^k_i \right) \right] \cdot \mathbf{t}^k_{ij}, \tag{7}$$

where r_{ij}^k is the position vector of that contact point from the center of mass of the i^{th} floe to the contact point at the k^{th} contact point. However, per friction laws there is a maximum magnitude limited by the coefficient of friction (Hopkins, 1996) such that

$$|\mathbf{F}_{ij,t}^k| \leq \mu |\mathbf{F}_{ij,n}^k|. \tag{8}$$

The presence of tangential forces leads to energy dissipation upon collisions.

3.5 Interactions with boundaries

Coastal boundaries are naturally prescribed as stationary polygonal floes, and an arbitrary number of such boundaries are possible if, for example, one is interested in simulating the sea ice in Fjords with many islands. The interaction forces with the coastal boundaries are calculated in a similar way as with other floes, but assuming that the elasticity of a boundary is infinite (i.e. all elastic deformation occurs within a floe). The frictional parameters with coastal boundaries could be different, although they are kept the same by default. Periodic boundary conditions could be used in addition to coastal boundaries in channel-type configurations. Periodic (and double-periodic) boundary conditions are achieved by using ghost floes (gray floes in Figure 3). The ghost floes are shifted copies of all floes that are close to one boundary and have the potential to overlap with the floes at the other boundary. The framework dealing with periodic boundary conditions is also directly applicable for parallel implementation as each processor could resolve its subdomain in physical space and exchange the information about the location of ghost floes at its edges with neighboring processors. This capability will be implemented in future versions of the code, but in its current form, the parallel computing is utilized by cores within a single node with Matlab's parfor loops.

4 Processes affecting floe shapes

4.1 Floe fractures

4.1.1 Defining the floe stress tensor

Stress and strain rates are important for physical processes such as fracture and lead formation. The collision function keeps track of the location and forces associated with each collision. We calculate the stress tensor of individual floes (Rothenburg & Selvadurai, 1981; André et al., 2013) via

$$\underline{\underline{\sigma_i}} = \frac{1}{2V_i} \sum_{j,k} f_{ij}^k \otimes r_{ij}^k + r_{ij}^k \otimes f_{ij}^k, \tag{9}$$

where f_{ij}^k is the force at the k^{th} contact point between the i^{th} and j^{th} floes and r_{ij} is the position vector of that contact point from the center of mass of the i^{th} floe to the contact point. Note that for non-convex elements, there could be multiple contact points, and hence k could be greater than one. The stress tensor is later used to define the floe fracture criteria. The continuous representation of the stress tensor over a coarse Eulerian grid is obtained by volume-weighted averaging of the stress tensors of the individual floes (Chang, 1988) within each grid box:

$$\underline{\underline{\sigma}}(x, y) = \frac{1}{V_{tot}} \sum_i \underline{\underline{\sigma_i}} V_i, \tag{10}$$

where the index i includes only floes with centers of mass located inside the coarse grid box at the location (x, y) and V_{tot} is the total volume those floes excluding the floe areas outside the grid box.

The homogenized stresses are be used in the following way, depending on the configuration of model parameterizations. The main usage revolves around defining the appropriate rule for fracturing individual floes based on local and/or non-local stress criteria. Specifically, it is straightforward to define fracture criteria based on, e.g., Mohr-Coulomb failure envelope (Figure 4) that is defined in the space of principal stresses of a floe stress tensor (Weiss & Schulson, 2009). The equation for the failure envelope boundaries are $\sigma_1 = q\sigma_2 + \sigma_c$ where $q = 5.2$ and $\sigma_c = 250$kPa. Other options for floe-fracture criteria could be derived from yield curves that are used in continuous models (Hibler, 1979). The connection with the SubZero model, where floes are rigid (nondeformable) objects, is that the macro-scale strain rate appears when floes are fracturing (or ridging/rafting). Thus, satisfying criteria for individual floe fractures would lead to macro-scale sea ice motion, which in continuous formulations is described by the presence of a yield curve. For example, in viscous-plastic sea ice rheology, an elliptical yield curve is used with a strength parameter $P = P^*h$ that is proportional to sea ice thickness h for fully ice-covered regions (Hibler, 1979). The values of P^* used in SubZero are provided in Table 1.

4.1.2 Fracture criteria based on homogenized floe stress

The basic isotropic fracture mechanism is implemented based on the stress experienced by floes and fractures a floe into a number of smaller pieces (Figure 6) when the principal stress values satisfy the specified fracture criteria (Figure 4). When it is determined that a fracture should occur, a floe is split into the desired number of elements via Voronoi tessellation based on random x and y points coordinates (uniform distribution) acting as centers of the Voronoi cells. The mass and momentum of the system are conserved after the floe fractures into smaller pieces. The number of elements into which the floe splits can be determined via a probabilistic process based on the proximity of the floe stress to the boundaries of the failure criteria. The shattered pieces form new floes that could continue braking until stresses are relieved. Note, without fracturing, the packed and interlocked floes would have no motion, and hence the motion occurs when the particle fracture criteria are satisfied. Therefore, one could draw connections between the concepts of the yield curve in continuum mechanics and the fracture criteria of the elements, but those would need to be constrained with floe-scale observations.

The basic fracture rule implemented in the model includes the Mohr's cone and the elliptical yield curve that was used in viscous-plastic rheology (Figure 4), and any other breakage criteria could be easily implemented. When the breaking criteria is satisfied, the floe shatters into three pieces by prescribing three randomly located points within the floe and using them for Voronoi tessellation to split the floe into several subfloes. This is a simple procedure leading to an isotropic distribution of fractures regardless of the direction of the principal stresses. For studies focusing on the analysis of linear kinematic features, it would be necessary to formulate more advanced anisotropic fracture rules or use bonds between floes; this is an ongoing area of model development and we envision enabling this capability in future versions of SubZero.

4.1.3 Corner grinding

Observations of older floe fields show a tendency to form rounder shapes through repeated interactions with other floes. The corner grinding process uses the contact overlap areas to determine whether a floe could have its corner fractured; the likelihood of this happening is proportional to OverlapArea/FloeArea. The model tracks the contact points during a collision with other floes, and if there is a contact point nearby, it is qualified to fracture. For a corner with angle α and adjacent sides of length l_1 and l_2, where l is the minimum of l_1 and l_2, at least one contact must be within the radius l of the corner. For each eligible corner of the polygon, a fracture probability is defined as 1-α/Anorm, where Anorm=360-180/N, and N is the total number of vertices. This way, the prob-

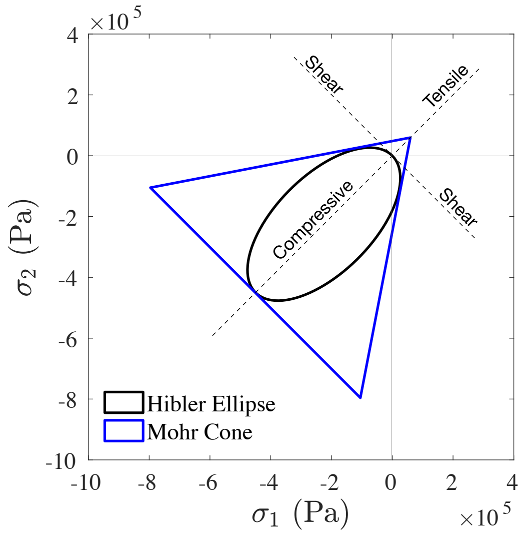

Figure 4. Examples of fracture criteria plotted as boundaries in the (σ_1, σ_2) space, including Mohr's cone and Hibler's ellipse. Floes for which homogenized stresses are large enough to reach (or temporarily exceed) the fracture rule boundaries end up fracturing into several elements. Those boundaries could be interpreted as yield curves for individual floes because only upon reaching those boundaries can there be any motion within the floe by means of fracturing it into smaller pieces.

ability of fracture increases as α approaches 0^o. For all floe corners that fracture, a triangle is defined with the same angle α and adjacent edges five times smaller than l. Figure 5 shows a floe field going through the corner fracture process. It can be seen that some of the sharper corners are broken off from 5a as the angles trend closer to that of a regular polygon. Figure 5b shows the rounded floes after many collisions, and the fractured pieces have been plotted with a dark gray color to distinguish them from the initial floes (colored with light gray).

4.2 Welding

We define welding as freezing of neighboring ice floes to form a bigger consolidated floe. An example of two floes welding together is shown in Figure 6. It is common for two ice floes to weld together when the temperature dips below freezing over the winter in the arctic. We imitate this process by using thermodynamic criteria to determine if two overlapping floes will weld together. When welding occurs, the properties of the newly created floe are determined by satisfying the mass, momentum, and angular momentum conservation laws. Our most straightforward parameterization defines the welding probability of a floe in contact with another floe as

$$P^i_{weld} = P_{F^i_{heat}} \frac{\delta A_{i,j}}{A^i} \tag{11}$$

where $\delta A_{i,j}$ is the overlap area between two floes, and the proportionality constant $P_{F^i_{heat}}$ is non-zero only when the ice is freezing. Improvements to this simple process could specify the probability to depend on the heat flux out of the ice floe if such a parameterization is informed by observations.

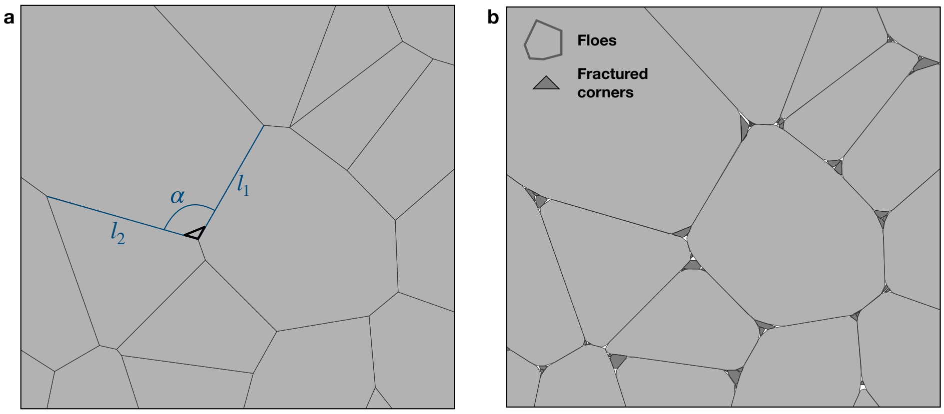

Figure 5. Example of a floes where the sharp corners are breaking off upon tight contact with other floes. **(a)** The initial intact floe configuration with fully-packed interacting floes. Denoted are a vertex angle, α, the lengths of adjacent edges, l_1 and l_2. The black line denotes the corner that will be fractured (isosceles triangle with the same angle α). **(b)** The state of the floes after the occurrence of multiple corner fractures. Fractured corners are modeled the same as regular floes but here they have been plotted with a dark gray color to distinguish from the initial floes that are colored with light gray.

4.3 Ridging and rafting

Sea ice can transfer mass from one floe to another through the ridging process. For this model, a critical thickness is set to determine if ridging or rafting is possible for two floes in contact (Parmerter, 1975). As long as at least one of the floes exceeds this threshold, then ridging will take place. When ridging occurs, the mass will transfer from one floe to the other, and the floe that loses mass will also have its area updated. If both floes exceed the critical thickness ($h_c = 0.25$), a probability function is set to determine the exchange of mass between the two floes

$$P_{Floe1} = \frac{1}{1 + h_1/h_2}, \tag{12}$$

where h_1 and h_2 are the thicknesses of the two floes undergoing ridging. If only one floe exceeds the thickness, then the thin floe loses its mass to the thicker floe. Floe properties are updated to ensure that the overall mass and momentum are conserved upon the adjustment of floe shapes (Figure 6). The ridging of sea ice can lead to complex sea ice shapes with a computationally prohibitive number of vertices. To reduce their complexity, we implement an algorithm that dynamically simplifies floe shapes (see Section 5.2).

When the two interacting floes are both below this critical thickness threshold ($h_c = 0.2$), they have a possibility of rafting where P_{raft} is a value set by the user. The numerical algorithm for the rafting process is similar to ridging, and mass will transfer from one floe to the other. After this rafting event, the floe that loses mass will also have its area updated. Floe properties are updated to ensure that mass and momentum are conserved throughout this operation. The updating of floe geometry is also similar to that shown in Figure 2.

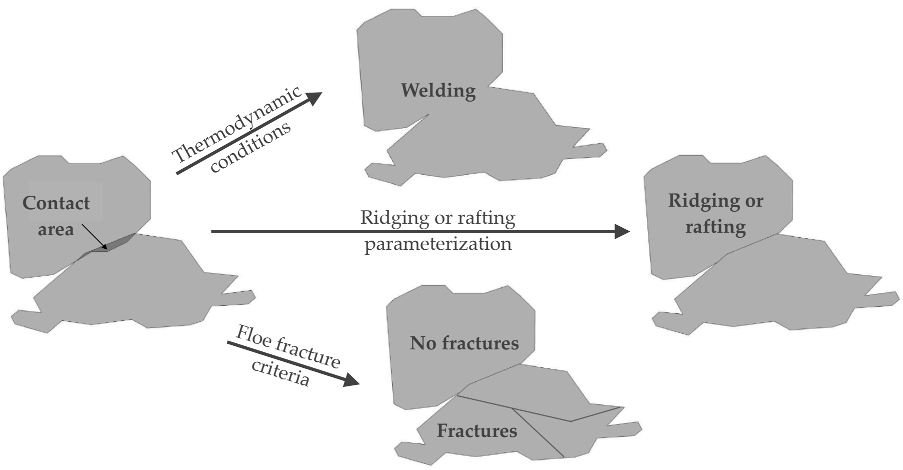

Figure 6. Example of two floes in contact leading to various possible outcomes, including welding, ridging/rafting, and fractures. The floe interaction forces are computed based on the geometry of the overlapping area. Collision forces define the homogenized floe stress tensor used in fracture parameterization that splits the floe into several pieces. Welding occurs if a thermodynamic criterion is satisfied and leads to the merger of two floes into one. The ridging/rafting parameterization determines if the overlap area between the floes will be absorbed into increasing the thickness of one of the two floes in contact.

4.4 Thermodynamic thickness changes

For existing floes, the basic version of the thermodynamic sea ice growth calculates the tendency of its thickness based on the net atmospheric and oceanic heat fluxes, and the tendency is inversely proportional to its thickness. This thickness growth assumes that the temperature inside the sea ice is always equilibrated to a linear profile, and the changing thickness is the only variable governing the heat flux. This basic version of the code is aimed at simulating sea ice mechanics, and hence the thermodynamic processes are simplified. Future thermodynamic schemes will include the option of using multi-layer thermodynamics and include the treatment of snow cover.

In open-ocean regions where there are no ice floes, and freezing conditions are satisfied, i.e., the surface ocean temperature is maintained at the freezing point, and the lost heat fluxes are partitioned into creating new floes with a prescribed minimum thickness. Thus, the total volume of new floes to be created in an open area together with the minimum floe thickness defines the total area of the new floes that are then generated using the packing algorithm.

For small-scale floes (about 100 m and smaller), lateral growth and melting can be important, and this capability will be implemented in future versions of the code.

5 Peculiarities of the numerical implementation

5.1 Tracking unresolved floes

Keeping track of all the small floes generated through the fracturing and ridging processes performed in the model becomes computationally expensive. Thus, a lower limit is set, at which point any floe with a smaller area is removed from the simulation and kept track of in a separate variable. The mass of all unresolved floes is stored in a variable on a coarse Eulerian grid. Utilizing the Eulerian sea ice velocity (see section 6.2), the dissolved ice mass is advected around the domain to preserve mass. Under proper thermodynamic conditions, this unresolved floe variable can act as a source for newly generated floes via section 3.2 conserving the mass of the system. In future versions of the model, parameterizations of the cumulative dynamical impact of small-scale unresolved sea ice will be used in the calculation of forces and torques on the remaining floes.

5.2 Dynamic simplification of floe boundaries

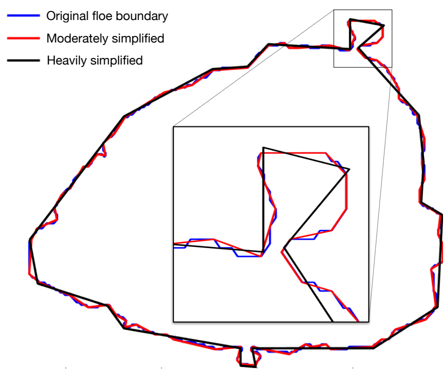

Figure 7. Example of a boundary simplification for a polygonal floe using the Douglas-Peucker algorithm. Initial floe boundary with 292 vertices (blue), its moderate simplification to 81 vertices (red), and heavy simplification to only 23 vertices (black). Inset shows a zoomed-in view of the protruding region at the top of the floe inside a black square box.

Certain processes in the numerical implementation (such as ridging, welding, and floe creation) lead to floes with a very large number of vertices, which is problematic for two reasons. First, when running simulations with large numbers of floes, this creates excessively large data structures which need to be stored. Secondly, performing operations such as rotating, translating, or calculating overlaps with other floes becomes computationally cumbersome. To avoid this, we use a Douglas-Peucker simplification algorithm to reduce the complexity of the shape. The floes retain qualitatively similar shapes as shown in Figure 7. After its simplification, the thickness of the floe is updated to conserve mass and momentum.

5.3 Parallel for-loops for multi-core processors

The SubZero program can run the collision algorithm, update floe trajectories, create new floe elements, weld floes, and fracture floes in parallel. To achieve this, we define for each given floe the potential interactions field that essentially copies all the necessary information about only those surrounding floes that have their bounding circles overlap with a given floe. The potential interactions are found as described in 3.4. The floe number, vertices, velocities, thickness, area, and centroid are all stored. This data is required to calculate the collisions between two floes and when two overlapping floes weld together independently of other rows in the floe structure. Updating floe trajectories and fracturing floes can be done in parallel and do not rely upon information from other floes in the structure. The creation of new elements and the welding algorithm divides the domain into smaller regions and bin the ice floes based on location. These subregions are then run in parallel.

Table 1. A list of key parameters used in the SubZero model, including their default numerical values, a brief description, and the processes that use these parameters.

Parameter	Description	Process
$E = 6 \times 10^6$ Pa	Young's Modulus	Floe Interactions
$G = \frac{E}{2(1+\nu)}$	Shear Modulus	
$\nu = 0.3$	Poisson's ratio	
$\mu = 0.3$	Coefficient of Friction	
N_{Frac}=75	Time steps between fracturing	Floe Fractures
$N_{Pieces} = 3$	Number of pieces for fracturing	
$P^* = 5{\times}10^3$ N m^{-1}	Floe strength-to-thickness ratio	
N_{cor}=10	Time steps between corner grinding	Corner Grinding
N_{Weld}=25	Time steps between welding	Floe Welding
F_{Weld}= 150	Welding probability coefficient	
$P_{ridge} = 0.1$	Ridging probability coefficient	Floe Ridging
$N_{pack} = 5500$	Time steps between floe creation	Floe Creation
$k = 2.14$ W m^{-1} K^{-1}	Thermal conductivity of surface ice layer	Floe Creation
$L = 2.93 \times 10^5$ J kg^{-1}	Latent heat of freezing	Floe Creation
$N_{simp} = 20$	Time steps between simplification of floe boundaries	Floe Simplification
$\rho_i = 920$ kg m^{-3}	Density of ice	Floe mass and moment of inertia
$\rho_a = 1.2$ kg m^{-3}	Density of air	Surface stresses
$\rho_o = 1027$ kg m^{-3}	Density of ocean	
$Cd_{atm} = 10^{-3}$	Atmosphere-ice drag coefficient	
$Cd_{ocn} = 3{\times}10^{-3}$	Ocean-ice drag coefficient	
$N_{MC} = 100$	Number of sample points for Monte Carlo integration over floe surface	
$\Delta t = 10$ s	Integration time step	Time-stepping
A_{min}= 2 km^2	Minimum area of resolved floes	Floe state
$N_b = 0$	Number of floes creating the boundary	Floe state

6 Coupling with ocean and atmosphere models on the Eulerian grid

6.1 Atmosphere and ocean forcing of individual floes

The atmospheric and oceanic equations of motion could be solved either within the Eulerian or Lagrangian frameworks. The coupling with the floe model occurs based upon the gridded representation of sea ice variables. For calculation of the oceanic and atmospheric stresses acting on individual floes, a Monte-Carlo surface integration method is used. Random points in space are assigned, and ocean and atmosphere flows are interpolated onto these points, after which stresses are computed. Less than about 100 points are needed for an accurate estimation of stresses, resulting in about 5% accuracy. The surface stresses and buoyancy fluxes that the ocean model is receiving from the sea ice model are computed by taking averages of the floe stresses and growth/melt rates over an Eulerian grid of the ocean model. This achieves a two-way coupling of both dynamic and thermodynamic components of the ocean and ice models. The same coupling can be arranged with the atmospheric model, and this capability would be implemented in the code as part of future developments.

6.2 Mapping the state of the floe model to the Eulerian grid

A coarse Eulerian grid is designated for the domain to diagnose the macroscale motion of the sea ice and couple it with Eulerian oceanic and atmospheric models. The domain is divided into smaller regions that align with this coarse spatial grid. Floes that overlap with any piece of the smaller boxes are identified, and the concentration is calculated first. Next, variables such as sea ice velocity and acceleration are calculated by scaling the contribution of individual floes by the mass of a floe present within the cell in question. Other variables such as the total force exerted on a coarse grid cell are not weighted by the mass of the floe experiencing the force.

7 Examples of simulated sea ice behavior

Here we present several test cases demonstrating the potential utility of the SubZero sea ice model. Specifically, we showcase simulations that highlight specific physics of the model, including the role of floe fractures in a pure compression experiment, the evolution of floe size distribution in a domain with complex coastline, and the wintertime simulation that includes all model physics.

7.1 Evolution of sea ice floes under large-scale compression

The behaviour of granular-type materials, including sea ice, are commonly tested using deformation experiments, e.g., subjecting the material to externally-imposed pure compression, tension, or shear. Here we demonstrate the behaviour of sea ice floes subject to large-scale compression, which is just one of the possible experiments that illustrates the non-standard formulation of the SubZero model. We start with a fully-packed sea ice domain and impose the motion of the North/South boundaries towards the center of the domain while keeping the East/West boundaries stationary. The boundaries move with a constant prescribed velocity, $v_b = 0.1$ m s^{-1}, and this leads to a reduction of the sea ice area and ensures convergent sea ice motion.

7.2 Summer sea ice motion through Nares Strait

The Nares Strait simulation demonstrates the role of floe fractures in wind-driven sea ice transport through narrow straits. The simulation aims to reflect spring or summer-like conditions of Arctic sea ice export through Nares Strait after the breakup of its winter arches. Due to floe jamming as they pass through the narrow constriction, the sea ice transport through the strait occurs in the form of episodic events (Kwok et al., 2010;

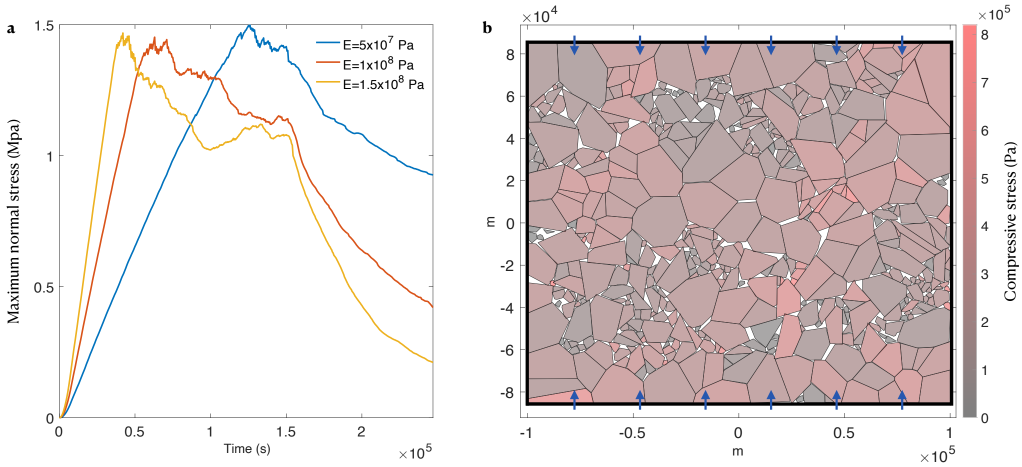

Figure 8. Evolution of sea ice under an idealized compression experiment. **(a)** Temporal evolution of the maximum normal stress averaged over an entire domain; the three curves represent simulations with different Young's moduli, E, prescribed for the floes. **(b)** The state of the floes at the end of the simulation with a reference value of Young's modulus of E=1.5 10^8 Pa, corresponding to the yellow curve in panel **(a)**. Blue arrows represent the imposed direction of motion of the top and bottom boundaries of the domain; the left and right boundaries remain stationary.

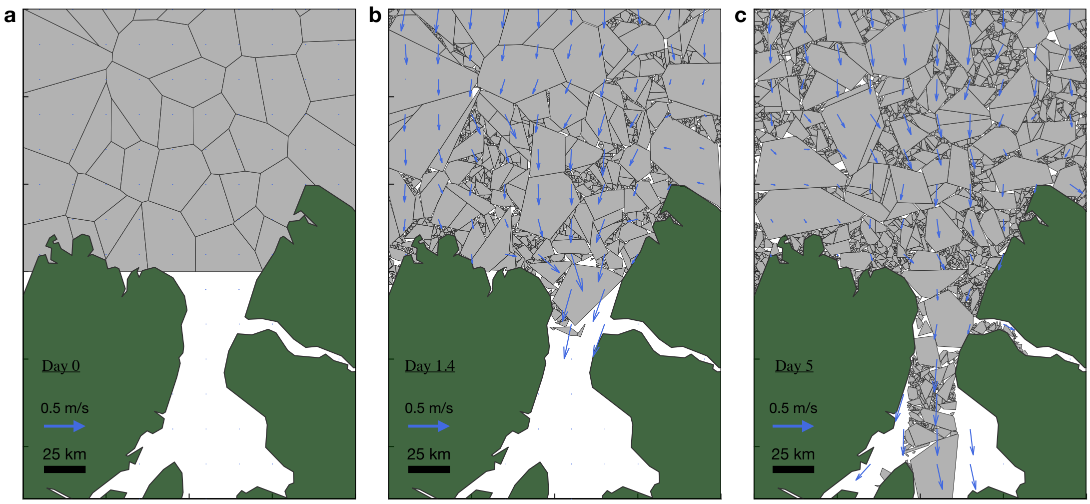

Figure 9. Evolution of sea ice floes as they pass through the Nares Strait, including **(a)** initial floe state, **(b)** floes shortly after sea ice breakup that occurred after about 1.4 days, and **(c)** floe state after 5 days when many floes have passed through the Nares Strait. The initial distribution of floes were generated using Voronoi tessellation and the subsequent evolution of floe shapes is only subject to floe fractures. Blue arrows represent sea ice velocity in a continuous sense, after averaging floe momentum within grid boxes of an Eulerian grid.

Moore et al., 2021). Since the transport events are relatively short (order of days and less), the effects of thermodynamic sea ice melt could be considered secondary relative to mechanical floe processes such as collisions and fractures. We thus initialize the model with relatively large floes of uniform thickness, covering only the area right ahead of the strait. The southward winds generate stresses that push the floes through the strait. The interactions between the floes and with coastal boundaries (treated as static floes) lead to floe fractures. To suppress the rapid creation of tiny floes due to frequent fractures, we set up the simulation to resolve only floes with an area greater than 1 km^2. In this basic model formulation, we assume that the unresolved small floes do not significantly affect the dynamics of larger floes, and the model only tracks their mass density using the Eulerian grid to ensure mass conservation. Note that in future more complex model formulations, the mass density could be used to parameterize the cumulative effect of small-scale floes on the dynamics of resolved floes.

As winds push the initially large floes through the strait, the frequent floe fractures quickly leads to an equilibrated floe size distribution (FSD), in just a few days (Fig. 10a). The number of floes grows from dozens initially to several thousands (Fig. 10b), but the FSD takes the form of a power-law distribution with an exponent close to -2. The FSD is free to equilibrate to a different power-law exponent (or not be a power law at all) depending on the forcing and floe interaction and fracture laws. In a winter-like simulation described in the next section, the FSD also equilibrates to a power-law distribution but with a different exponent. Power-laws in FSDs have been commonly reported based on observations in various Arctic Ocean regions, with exponents ranging from about -3 to -1 (D. Rothrock & Thorndike, 1984; Holt & Martin, 2001; Denton & Timmermans, 2021). A recent study using very high-resolution images demonstrates that within a wide range of floe sizes, the power-law exponent for the area-based FSD belongs to an approximate range from (-2, -1.65), which translates to a range of slopes (-3, -2.3) if size as the square root of the area is used to define FSD (Denton & Timmermans, 2021). Our simulation with fractures only driven by mechanical floe interactions gives an exponent of about -2, comparing reasonably well with various observations especially given that the model has not been specifically tuned to reproduce neither FSD or ITD.

As the sea ice breaks into smaller floes, they can propagate through the relatively narrow strait. The sea ice mass flux through the strait is not smooth as floes often jam in narrow constrictions (Fig. 10b). The jamming occurs when relatively large floes cluster in narrow parts of the strait, and sea ice can only move after some of those floes break into smaller pieces. The breaking of floes depends on the fracture criteria; an ellipse was used for this simulation to conceptually mimic Hibler's elliptical yield curve that was used in continuous viscous-plastic sea-ice models (Fig. 10c). Floes that have stresses lying inside an ellipse do not break, and those who are on the ellipse or just outside of it do end up fracturing. These floe fractures lead to intermittent but large fluxes of sea ice area and transported mass (Fig. 10c). The sea ice area fluxes in Nares Strait estimated using satellite and flux-gate observations are of the order $O(10^3)$ km^2/day (Kwok et al., 2010; Moore et al., 2021) and generally agree with the idealized simulation with $O(10^3)$ km^2/day for relatively rare high-transport events and about $O(10^2)$ km^2/day for more frequent events. Thus, the idealized SubZero experiments are capable of qualitatively simulating many aspects of sea ice dynamics. However, its parameterization still requires tuning using floe-scale observations. We expect that observational estimates of FSD and mass fluxes inside Nares Strait and the driving forces such as wind stress and boundary stresses would be crucial for constraining floe collision and fracture parameterizations. Winter-time sea ice dynamics in the Nares Strait also present a crucial case study as sea ice can form arches that temporarily shut down its transport. This experiment is left for future studies, and we expect that it can be used to tune the balance between welding processes that bond floes together and fractures that break them apart.

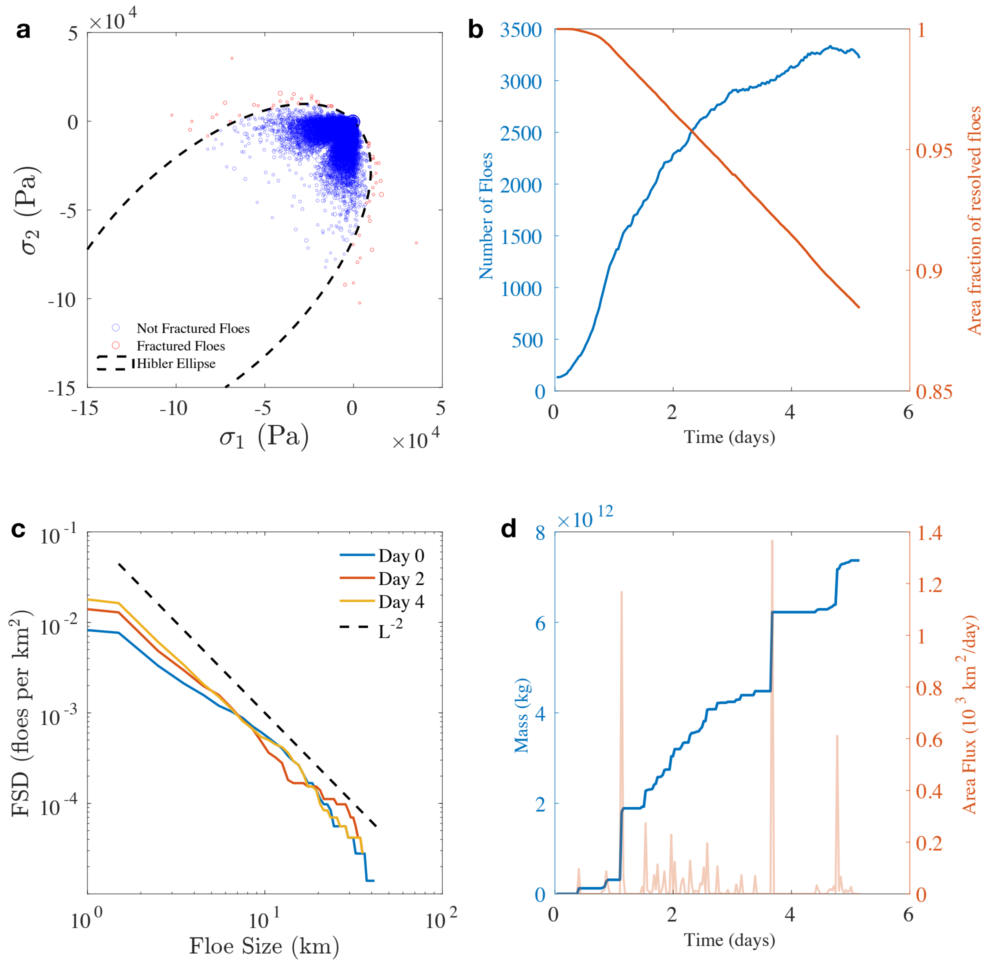

Figure 10. The evolution of the Nares Strait simulation. **(a)** Principle components of the homogenized floe stresses, with floes categorized by those that will experience fracture (red) and those that will not (blue). The black dashed curve represents a boundary for floe fracturing, in this case an ellipse similar to a yield curve used in viscous-plastic sea ice rheology. **(b)** Number of resolved floes and the fractional area that they occupy in the domain; note, the individual dynamics of floes that are too small is not simulated by the model but the cumulative area and volume of unresolved floes is being tracked. **(c)** Floe size distributions for sea ice floes that are inside the Nares Strait. **(d)** The cumulative sea ice mass transport through the northern entrance to the Nares Strait (blue) and the corresponding area flux (red).

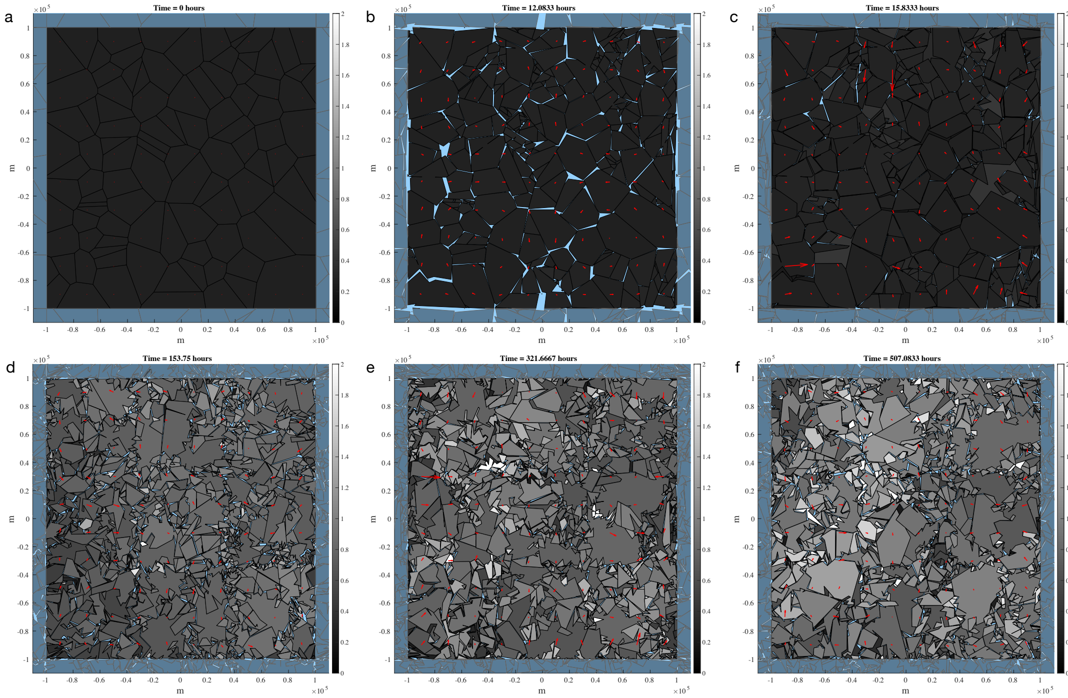

Figure 11. Evolution of sea ice during the winter-like simulation of sea ice growth with full physics of the model enabled. Panels **a-f** correspond to snapshots of floes and their thicknesses (shown with gray scale color bar) at model times denoted in the panel titles.

7.3 Winter ITD and FSD equilibration

Here we demonstrate an essential case of model equilibration in winter-like conditions, where all parameterizations are active. For a unique model like SubZero that simulates time-evolving floe shapes and has a freely-evolving number of floes, it is of particular interest to explore if the FSD and ITD equilibrate to distributions resembling observations. We subject sea ice to strong mechanical and thermodynamic forcing to facilitate an accelerated model evolution away from the initialized floe shapes, sizes, and thicknesses towards typical winter-like distributions. Specifically, we prescribe idealized ice-ocean stresses in the form of four equal-strength counter-rotating gyres (arranged like mechanical gears) that create relative sea ice motion and facilitate floe fractures and ridging. Alternatively, one could prescribe atmosphere-ocean stresses to achieve the same goal. To make this a winter-like simulation, we ensured a continuous sea ice growth by specifying a fixed negative heat flux that increases the thickness of existing ice floes, the formation of new ice floes in open ocean regions, and welding between floes. This idealized setup is aimed to demonstrate the evolution of floe shapes, sizes, and thickness under strong mechanical and thermodynamic forcing. We initialized the model with a fully-packed domain in which floes are cells of the Voronoi tessellation, all having the same thickness of 0.25 m and similar sizes (Fig. 11). These initial floe thickness and size distributions are highly unrealistic. Below we describe how the dependence on these initial conditions is lost as the simulation progresses and how the emerging distributions start resembling the observed ones.

In the early times of the simulation (within the first days), floe fractures and ridging/rafting processes lead to rapid changes in ITD and FSD (Fig. 12). The floe fractures form smaller floes, and this process establishes an approximate power-law distribution

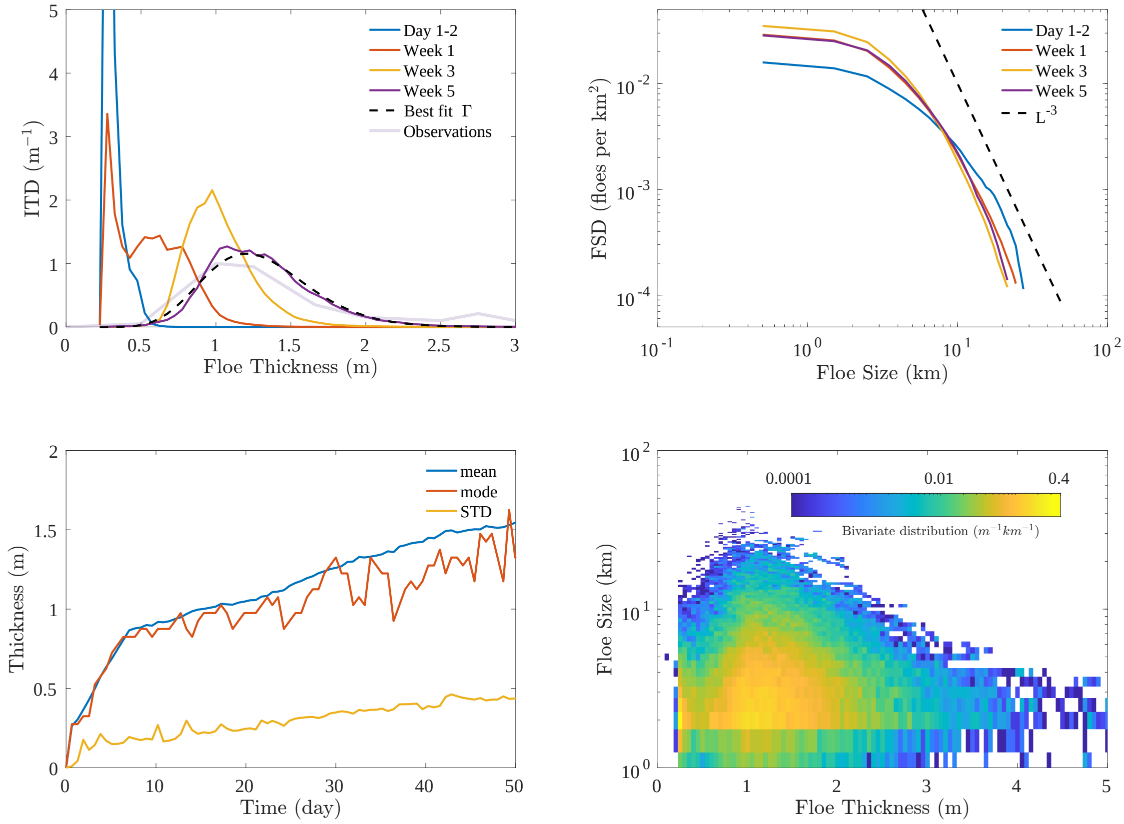

Figure 12. The evolution of floe size and thickness distributions for the winter simulation. **(a)** Ice thickness distribution (ITD) achieved in the early time after the initialization (blue), intermediate time (red), and at the end of the model simulation (orange); the best-fit gamma function is plotted for reference (dashed black line). **(b)** Floe size distribution (FSD), plotted as the number of floes in a particular size bin per square kilometer; the L^{-3} power-law, L being the floe size, is shown for reference (dashed line). Note, floes smaller than 2 km are not resolved in the simulation and only appear in the model as short-lived floes of recently fractured of larger floes. **(c)** Time evolution of the ITD mean, mode, and standard deviation. **(d)** Bivariate probability distribution of floes sizes and thicknesses, plotted for week 4 of the simulation.

in the range of resolved floes, which are larger than a few km. The ice-free areas open up due to ridging/rafting, and new ice floes are formed there and consequently participate in all processes. Note, the simulation is set to resolve floes with size above a certain threshold, which we set to 1km for this simulation. After about a week, the power-law exponent of the FSD equilibrates to a value of about -3, and the FSD starts resembling observations. Power laws in FSD are commonly found in various types of satellite sea ice observations, with the -3 exponent being well within the range of reported values (D. A. Rothrock & Thorndike, 1984; Stern et al., 2018). A recent study that used high-resolution sea ice imagery found the FSD power law to change within an approximate range of (-3, -2.2), using the square root of the area to define floe size. Notably, our model simulation equilibrated to an approximate -3 power-law having only internal sea ice interactions as a cause of fractures. However, in marginal ice zones (regions where FSDs are often computed from observations), floes are also fractured by surface waves (Montiel & Squire, 2017) – a process that is not yet included in our model. Since the inclusion of waves would preferentially create smaller-scale floes, the FSD might have a steeper slope, making the power-law exponent closer to the observations. But before the wave fracture parameterization is included, our simulation can be considered applicable for conditions in pack ice, away from marginal ice zones.

The ITD also departs rapidly from the initial delta function distribution (all floes were initialized with the same thickness). By the end of the first week, the ITD takes the form of a double-peak distribution, with a secondary minor peak emerging at around 0.6 m due to ridging processes (Fig. 12a). However, as time progresses, the secondary peak gets smeared out because many different ice thickness categories are ridged with each other. By the end of the month, the ITD takes a form of a smooth, single peak distribution with a pronounced asymmetric tail for thick ice. The ITD continues to move towards thicker sea ice because of the thermodynamic growth, while the tail of the distribution and its asymmetry increase due to ridging (Fig. 12c). At this stage, the dependence on the initially-prescribed ITD shape is lost, but the equilibrium is not reached as the ice continues to grow. Note that to acheive an equilibrated ITDs, the simulation would need to be run over multiple seasonal cycles, with winter-like sea ice growth followed by summer-like melt. Nonetheless, we can still evaluate if these transient ITDs resemble winter-time observations, at least qualitatively. The observed ITD is known to have an asymmetric shape that has been theoretically described using a gamma function distribution (Toppaladoddi & Wettlaufer, 2015) and the simulated ITD also resembles the gamma function distribution (Fig. 12a, dashed line). While the shape of the ITD resembles observations, some of its quantitative metrics do not compare well. Specifically, Arctic-wide satellite-deduced FSD for a winter month, like February, has a mean of 1.7 m and standard deviation of 0.77 m (Kwok et al., 2020). The ITD reaches a similar mean of about 1.5 m, but the standard deviation is only about 0.4 m, significantly lower than observations. Of course, our model simulation is highly idealized, and the resulting ITD would depend on the imposed mechanical and thermodynamic forcing and model parameters, all of which could be tuned for a better match with observations. However, another reason for the mismatch is that the observed ITD is composed of sea ice that is a mixture of first-year ice and multiyear ice, with a ratio of about 1.4:1 in February, while our model simulation only has first-year ice as it is run for a short amount of time. Since multiyear ice is typically thicker than first-year ice, its presence skews the ITD towards higher thicknesses and contributes to its large standard deviation. Considering these factors, the simulated ITD can be considered to be in qualitative agreement with observations. With a more elaborate experimental design, it might be possible to reach a quantitative agreement. Since this paper aims to introduce general SubZero capabilities, we envision many crucial process studies performed by the broader sea ice modeling community.

8 Summary and Discussion

We constructed a model of sea ice floes that treats them as discrete polygonal elements. Its main advantage, and the key difference from existing sea ice DEMs, is that SubZero's elements can change their shapes due to parameterized processes such as welding, fracturing, ridging, etc. Existing sea ice DEMs use fixed-shape elements (e.g., disks, rectangles, or tetrahedra), and this can limit the interpretation of the model state when it comes to defining individual floes for comparison with data. Our model aims to bridge this gap and provide a framework that can be directly used to predict sea ice floe motion, either collectively in the form of floe size or thickness distributions or individually for each floe.

We tested SubZero in several idealized scenarios to demonstrate its capabilities as a model of a granular and brittle material (the summer-time Nares Strait simulation) and a model with an active creation of new elements in addition to welding and fracture mechanics (the winter-time simulation). In both scenarios with idealized forcing and boundary conditions, the model generated FSD with a power-law exponent ranging from about -2 (for pure fractures) to -3 for winter-like simulation. Both power-law exponents are well within the observed range. Similarly, during the winter-time sea ice growth simulations, the ice thickness distribution approached a qualitatively similar shape to the observed distribution, consisting of a single peak and an asymmetric tail for thicker sea ice. Since the model formulation specifies only the rules of floe interactions, one cannot guarantee that sensible equilibrated floe size and thickness distributions would emerge or that those would even remotely resemble the observed distributions. Yet, including only core processes with minimal parameter adjustment and using highly-idealized forcing and boundary conditions, the model approached a regime that resembles the observed sea ice behavior. This qualitative, and for many metrics, quantitative, consistency with observations provides a substantial rationale for exploring various improvements to model physics. In particular, given its ability to explicitly simulate the floe lifecycle, the philosophy behind SubZero strives to create a new generation of sea ice models.

We presented a proof of concept of a DEM with a varying number of elements that can change their shapes subject to parameterized floe-scale physics. While the SubZero model already exhibits behavior consistent with sea ice observations, several improvements need to be made for it to become an operational sea ice model. Specifically, we expect that a more realistic formation of linear kinematic features could be achieved by developing anisotropic floe fracture parameterizations, which would be an essential step toward mimicking floe-scale sea ice deformation. Another drawback of our model, and DEMs in general, is that its improved realism of floe dynamics is computationally demanding, and running such a model on basin scales presents a significant challenge. This issue could be addressed by improving the computational speed of the code using high-performance languages and GPU-enabled architectures. However, there will always be a limit to computing capabilities. Hence, to facilitate more accessible research and faster progress, developing computationally cheap basin-scale models would be necessary. One could envision theoretical studies attempting to formulate rescaled floe interaction rules such that floes in the model would effectively represent clusters of floes of a particular scale. The problem of rescaling the floe interaction rules is tightly linked to the issue of representing the impact of unresolved floes and quantitatively defining what a floe represents in physical space. Nonetheless, even in its present prototype-like state, we see SubZero as an attractive new sea ice model that could be valuable for idealized process studies and regional sea-ice simulations.

We now comment on key distinctions of SubZero from existing continuous and discrete element sea ice models. Continuous rheology models, like viscous-plastic models (Hibler, 1979), are meant to represent basin-scale sea ice motion and are formulated for lengthscales larger than about 10–100 km to represent characteristics averaged over a large number of floes. Unlike the SubZero sea ice model, continuous rheology models do not provide direct information about the positions, sizes, and shapes of individual floes, but they could provide statistical information such as FSD and ITD by solving their evolution equations subject to parameterized physics. SubZero's output also can be presented in the form of Eulerian sea ice variables, like velocity or concentration. However, it is not a given that this discrete element model has equivalent continuous rheology describing the evolution of its Eulerian diagnostics. Hence, significant questions remain about using DEMs like SubZero to improve continuous sea ice models.

Comparing SubZero to existing sea ice DEMs, we can point out some key differences. A general concept behind DEMS is to use pre-defined element shapes (such as points, disks, rectangles, or tetrahedra) to simplify calculations of collisions. More complex structures can be formed as clusters of simple elements that are bonded together. But this comes at the expense of computing forces for those bonds, which is typically a stiff problem requiring small integration time steps. Consequently, it is challenging to use existing sea ice DEMs for long-term simulations to study equilibrium sea ice distributions (such as FSDs and ITDs). Instead, such models are commonly used to address problems where the sea ice state does not dramatically evolve from initial conditions, i.e., initial-value problems. SubZero bypasses the issue of using a large number of stiffly-connected simple elements by using complex floes with convex time-dependent shapes. Using complex floe shapes allows a straightforward creation of new elements in complex open-ocean regions between existing floes and simulating conditions with 100% ice cover using a modest number of floes. However, reducing the number of elements by transitioning to complex non-convex element shapes results in increased computational expense for resolving collisions and the need to parameterize floe-scale processes such as fractures and ridging. Parameterizations for the floe-scale processes could be derived by using the SubZero model by setting it up to resolve the sub-floe dynamics within individual floes; this approach is similar to nested runs used for resolving small-scale oceanic or atmospheric processes. The rationale behind SubZero's formulation is that it might be sufficient to use parameterized floe fractures and ridging (instead of explicitly resolving them) because these processes occur with high frequency and at a wide range of scales due to the highly varying and strong wind forcing typical for the Arctic Ocean. When only statistical behavior of sea ice floes is of interest and exact details of individual fractures and ridging are not, then a model like SubZero can effectively perform regional simulations of sea ice behavior at seasonal scales. Thus, SubZero demonstrates a new approach to floe-resolving sea ice modeling, being distinct from existing continuous and discrete element sea ice models. How the unique capabilities of the SubZero model could lead to our improved understanding of sea ice dynamics remains to be demonstrated in future studies.

9 Code Availability

The SubZero code (Manucharyan & Montemuro, 2022) is provided at the public GitHub repository `https://github.com/ONR-MURI/FloeModel-Matlab/tree/Published`.

Acknowledgments

G.E.M and B.P.M gratefully acknowledge support from the Office of Naval Research (ONR) grant N00014-19-1-2421. The authors highly appreciate the insightful discussions at the online workshop "Modeling the Granular Nature of Sea Ice" organized by the School of Oceanography, University of Washington as part of the ONR MURI project N00014-19-1-2421.

References

André, D., Jebahi, M., Iordanoff, I., luc Charles, J., & Néauport, J. (2013). Using the discrete element method to simulate brittle fracture in the indentation of a silica glass with a blunt indenter. *Computer Methods in Applied Mechanics and Engineering*, *265*, 136-147. doi: https://doi.org/10.1016/j.cma.2013.06.008

Chang, C. (1988). *Deformation behavior of sands under cyclic loading - a micro-structural approach* (Tech. Rep.). United States Air Force Office of Scientific Research.

Chen, N., Fu, S., & Manucharyan, G. (2021a). Lagrangian data assimilation and parameter estimation of an idealized sea ice discrete element model. *Journal of Advances in Modeling Earth Systems*, *13*(10), e2021MS002513.

Chen, N., Fu, S., & Manucharyan, G. (2021b). Lagrangian data assimilation and parameter estimation of an idealized sea ice discrete element model. *Journal of Advances in Modeling Earth Systems*, *13*(10), e2021MS002513. (e2021MS002513 2021MS002513) doi: https://doi.org/10.1029/2021MS002513

Cox, G., & Weeks, W. (1988). Numerical simulations of the profile properties of undeformed first-year sea ice during the growth season. *Journal of Geophysical Research: Oceans*, *93*(C10), 12449–12460.

Cundall, P. A., & Strack, O. D. (1979). A discrete numerical model for granular assemblies. *geotechnique*, *29*(1), 47–65.

Damsgaard, A., Adcroft, A., & Sergienko, O. (2018). Application of discrete element methods to approximate sea ice dynamics. *Journal of Advances in Modeling Earth Systems*, *10*(9), 2228–2244.

Denton, A. A., & Timmermans, M.-L. (2021). Characterizing the sea-ice floe size distribution in the canada basin from high-resolution optical satellite imagery. *The Cryosphere Discussions*, *2021*, 1–20. doi: 10.5194/tc-2021-368

Feng, Y., Han, K., & Owen, D. (2012). Energy-conserving contact interaction models for arbitrarily shaped discrete elements. *Computer Methods in Applied Mechanics and Engineering*, *205-208*, 169-177. (Special Issue on Advances in Computational Methods in Contact Mechanics) doi: https://doi.org/10.1016/j.cma.2011.02.010

Gutfraind, R., & Savage, S. B. (1997). Smoothed particle hydrodynamics for the simulation of broken-ice fields: Mohr–coulomb-type rheology and frictional boundary conditions. *Journal of Computational Physics*, *134*(2), 203–215.

Herman, A. (2013). Numerical modeling of force and contact networks in fragmented sea ice. *Annals of Glaciology*, *54*(62), 114–120. doi: 10.3189/2013AoG62A055

Herman, A. (2016). Discrete-element bonded-particle sea ice model design, version 1.3 a–model description and implementation. *Geoscientific Model Development*, *9*(3), 1219–1241.

Herman, A., Cheng, S., & Shen, H. H. (2019). Wave energy attenuation in fields of colliding ice floes–part 1: Discrete-element modelling of dissipation due to ice–water drag. *The Cryosphere*, *13*(11), 2887–2900.

Hibler, W. D. (1979). A dynamic thermodynamic sea ice model. *Journal of physical oceanography*, *9*(4), 815–846.

Hibler III, W., & Schulson, E. M. (2000). On modeling the anisotropic failure and flow of flawed sea ice. *Journal of Geophysical Research: Oceans*, *105*(C7), 17105–17120.

Holt, B., & Martin, S. (2001). The effect of a storm on the 1992 summer sea ice cover of the beaufort, chukchi, and east siberian seas. *Journal of Geophysical Research: Oceans*, *106*(C1), 1017–1032.

Hopkins, M. A. (1996). On the mesoscale interaction of lead ice and floes. *Journal of Geophysical Research: Oceans*, *101*(C8), 18315-18326. doi: https://doi.org/10.1029/96JC01689

Hopkins, M. A., Frankenstein, S., & Thorndike, A. S. (2004). Formation of an aggregate scale in arctic sea ice. *Journal of Geophysical Research: Oceans*, *109*(C1).

Hunke, E. C., & Dukowicz, J. K. (1997). An elastic–viscous–plastic model for sea ice dynamics. *Journal of physical oceanography*, *27*(9), 1849–1867.

Hutchings, J. K., Roberts, A., Geiger, C. A., & Richter-Menge, J. (2011). Spatial and temporal characterization of sea-ice deformation. *Annals of Glaciology*, *52*(57), 360–368.

Hutter, N., Bouchat, A., Dupont, F., Dukhovskoy, D., Koldunov, N., Lee, Y. J., ... others (2022). Sea ice rheology experiment (sirex): 2. evaluating linear kinematic features in high-resolution sea ice simulations. *Journal of Geophysical Research: Oceans*, *127*(4), e2021JC017666.

Hutter, N., & Losch, M. (2020). Feature-based comparison of sea ice deformation in lead-permitting sea ice simulations. *The Cryosphere*, *14*(1), 93–113.

Kawamoto, R., Andò, E., Viggiani, G., & Andrade, J. E. (2016). Level set discrete element method for three-dimensional computations with triaxial case study. *Journal of the Mechanics and Physics of Solids*, *91*, 1–13.

Kulchitsky, A., Hutchings, J., Johnson, J., & Lewis, B. (2017). *Siku sea ice discrete element method model* (Tech. Rep.). University of Alaska Fairbanks and Oregon State University.

Kwok, R., Kacimi, S., Webster, M., Kurtz, N., & Petty, A. (2020). Arctic snow depth and sea ice thickness from icesat-2 and cryosat-2 freeboards: A first examination. *Journal of Geophysical Research: Oceans*, *125*(3), e2019JC016008. doi: https://doi.org/10.1029/2019JC016008

Kwok, R., Toudal Pedersen, L., Gudmandsen, P., & Pang, S. S. (2010). Large sea ice outflow into the nares strait in 2007. *Geophysical Research Letters*, *37*(3). doi: https://doi.org/10.1029/2009GL041872

Lindsay, R., & Stern, H. (2004). A new lagrangian model of arctic sea ice. *Journal of physical oceanography*, *34*(1), 272–283.

Liu, L., & Ji, S. (2018). Ice load on floating structure simulated with dilated polyhedral discrete element method in broken ice field. *Applied Ocean Research*, *75*, 53–65.

Manucharyan, G., & Montemuro, B. (2022). *Subzero sea ice model.* `https://github.com/ONR-MURI/FloeModel-Matlab/tree/Published`. GitHub.

Mehlmann, C., Danilov, S., Losch, M., Lemieux, J.-F., Hutter, N., Richter, T., ... Korn, P. (2021). Simulating linear kinematic features in viscous-plastic sea ice models on quadrilateral and triangular grids with different variable staggering. *Journal of Advances in Modeling Earth Systems*, *13*(11), e2021MS002523.

Mohammadi-Aragh, M., Losch, M., & Goessling, H. F. (2020). Comparing arctic sea ice model simulations to satellite observations by multiscale directional analysis of linear kinematic features. *Monthly Weather Review*, *148*(8), 3287–3303.

Monaghan, J. J. (1992). Smoothed particle hydrodynamics. *Annual review of astronomy and astrophysics*, *30*(1), 543–574.

Montiel, F., & Squire, V. A. (2017). Modelling wave-induced sea ice break-up in the marginal ice zone. *Proceedings of the Royal Society A: Mathematical, Physical and Engineering Sciences*, *473*(2206), 20170258.

Moore, G., Howell, S., Brady, M., Xu, X., & McNeil, K. (2021). Anomalous collapses of nares strait ice arches leads to enhanced export of arctic sea ice. *Nature communications*, *12*(1), 1–8.

Parmerter, R. R. (1975). A model of simple rafting in sea ice. *Journal of Geophysical Research (1896-1977)*, *80*(15), 1948-1952. doi: https://doi.org/10.1029/JC080i015p01948

Potyondy, D. O., & Cundall, P. (2004). A bonded-particle model for rock. *International journal of rock mechanics and mining sciences*, *41*(8), 1329–1364.

Rampal, P., Bouillon, S., Ólason, E., & Morlighem, M. (2016). nextsim: a new lagrangian sea ice model. *The Cryosphere*, *10*(3), 1055–1073.

Rothenburg, L., & Selvadurai, A. (1981). A micromechanical definition of the cauchy stress tensor for particulate media. *Mechanics of structured media : proceed-*

ings of the International symposium on the Mechanical Behaviour of Structured Media, *b*, 469-486.
Rothrock, D., & Thorndike, A. (1984). Measuring the sea ice floe size distribution. *Journal of Geophysical Research: Oceans*, *89*(C4), 6477–6486.
Rothrock, D. A., & Thorndike, A. S. (1984). Measuring the sea ice floe size distribution. *Journal of Geophysical Research: Oceans*, *89*(C4), 6477-6486. doi: https://doi.org/10.1029/JC089iC04p06477
Stern, H. L., Schweiger, A. J., Zhang, J., & Steele, M. (2018, 07). On reconciling disparate studies of the sea-ice floe size distribution. *Elementa: Science of the Anthropocene*, *6*. doi: 10.1525/elementa.304
Toppaladoddi, S., & Wettlaufer, J. S. (2015, Oct). Theory of the sea ice thickness distribution. *Phys. Rev. Lett.*, *115*, 148501. doi: 10.1103/PhysRevLett.115.148501
Tuhkuri, J., & Polojärvi, A. (2018). A review of discrete element simulation of ice–structure interaction. *Philosophical Transactions of the Royal Society A: Mathematical, Physical and Engineering Sciences*, *376*(2129), 20170335.
Turner, A. K., Peterson, K. J., & Bolintineanu, D. (2022). Geometric remapping of particle distributions in the discrete element model for sea ice (demsi v0. 0). *Geoscientific Model Development*, *15*(5), 1953–1970.
Weiss, J., & Schulson, E. M. (2009, oct). Coulombic faulting from the grain scale to the geophysical scale: lessons from ice. *Journal of Physics D: Applied Physics*, *42*(21), 214017. doi: 10.1088/0022-3727/42/21/214017
West, B., O'Connor, D., Parno, M., Krackow, M., & Polashenski, C. (2021). Bonded discrete element simulations of sea ice with non-local failure: Applications to nares strait. *Journal of Advances in Modeling Earth Systems*, e2021MS002614.
Wilchinsky, A. V., Feltham, D. L., & Hopkins, M. A. (2010). Effect of shear rupture on aggregate scale formation in sea ice. *Journal of Geophysical Research: Oceans*, *115*(C10).
Zhang, J., Schweiger, A., Steele, M., & Stern, H. (2015). Sea ice floe size distribution in the marginal ice zone: T heory and numerical experiments. *Journal of Geophysical Research: Oceans*, *120*(5), 3484–3498.